

Supporting Information

**Polymer Nanocomposites with High Energy Density and Improved Charge-discharge Efficiency Utilizing Hierarchically-structured Nanofillers**

Yushu Li, Yao Zhou, Yujie, Zhu, Sang Cheng, Chao Yuan, Jun Hu, Jinliang He and Qi Li\*

State Key Laboratory of Power System, Department of Electrical Engineering, Tsinghua University, Beijing 100084, China

E-mail: [qili1020@tsinghua.edu.cn](mailto:qili1020@tsinghua.edu.cn)

Keywords: dielectric, polymer nanocomposites, discharged energy density, charge-discharge efficiency

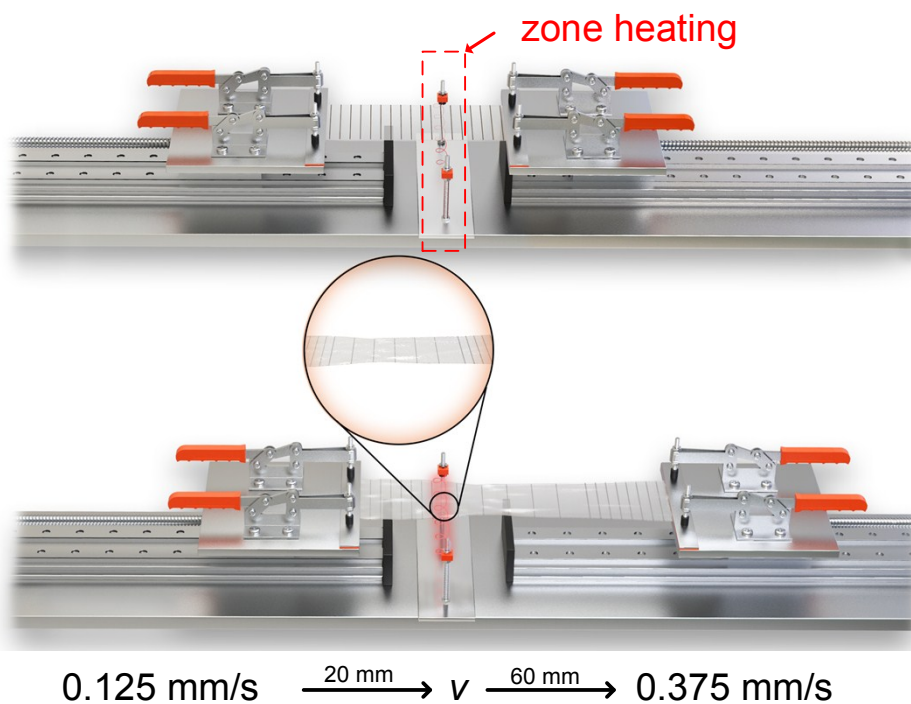


**Figure S1.** Schematic of the polymer film zone stretching machine.

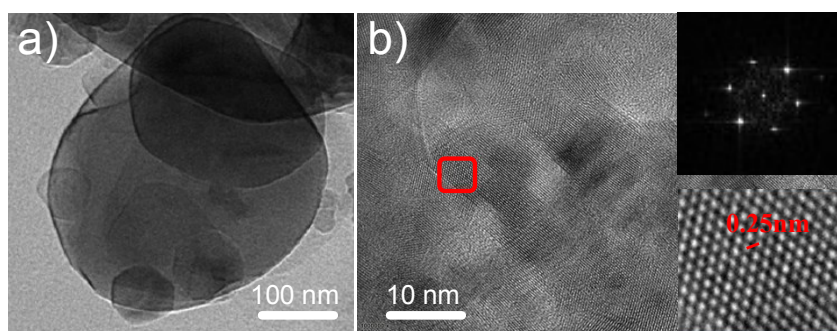


**Figure S2.** (a) TEM image of the individual free standing BNNS. (b) High-resolution TEM (HRTEM) image of BNNS. Inset, corresponding fast Fourier transform (FFT) and the electron diffraction pattern displaying a hexagonal symmetry structure.

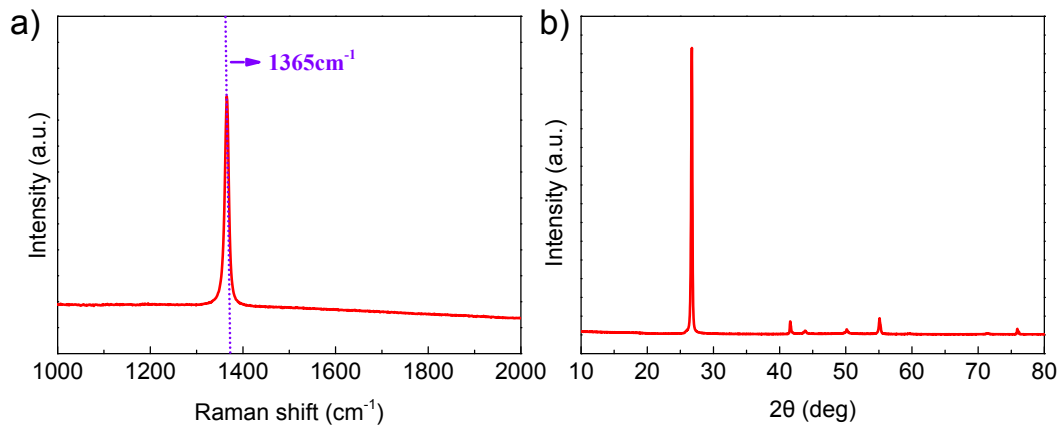


**Figure S3.** (a) Raman and (b) XRD spectra of BNNs. The Raman spectrum of BNNs presents a dominant peak near 1365 cm<sup>-1</sup> which can be assigned to the  $E_{2g}$  vibration of *h*-BN.

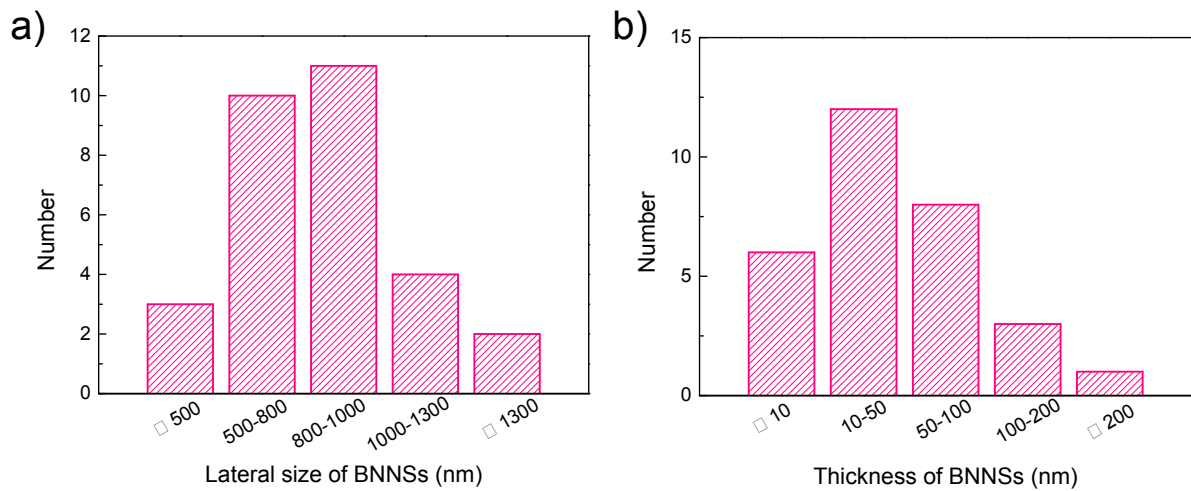


**Figure S4.** Statistical analysis on the (a) lateral size and (b) thickness of BNNs.

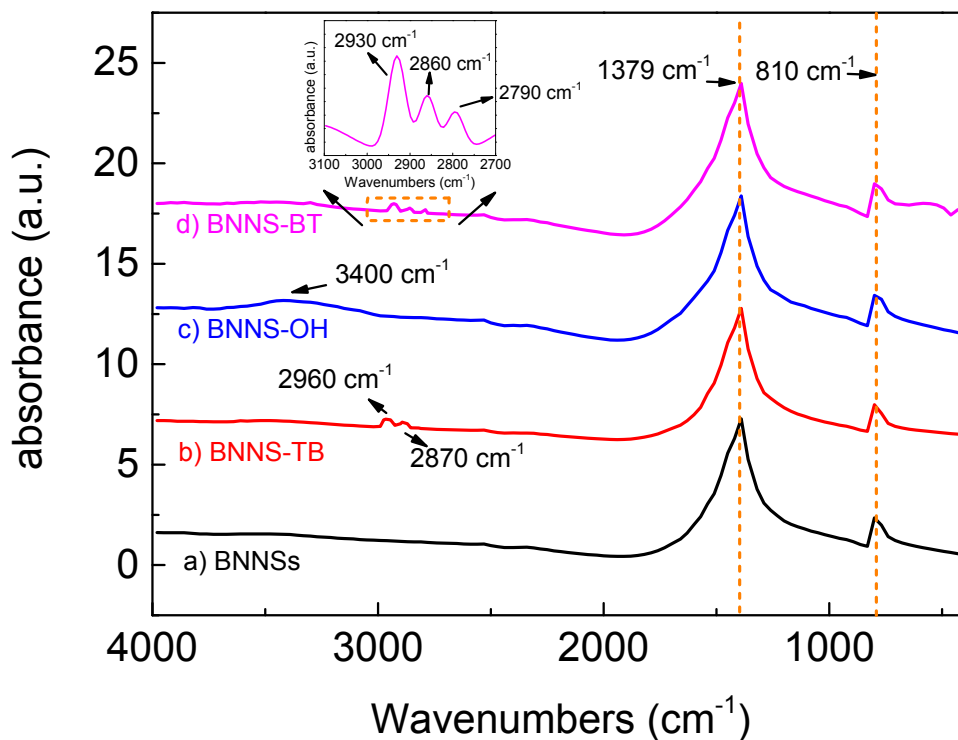


**Figure S5.** The Fourier transform infrared (FTIR) spectroscopy of the grafting process for BNNS-BT. The appearance of the C-H stretching vibration at  $2960\text{ cm}^{-1}$  and  $2870\text{ cm}^{-1}$  indicates the introduction of *tert*-butoxy groups on BNNS-TB. The disappearance of the O-H stretching at  $3400\text{ cm}^{-1}$  and the presence of C-H stretching at  $2930\text{ cm}^{-1}$  and  $2860\text{ cm}^{-1}$  in BNNS-BT indicate the grafting of BT onto BNNSs.

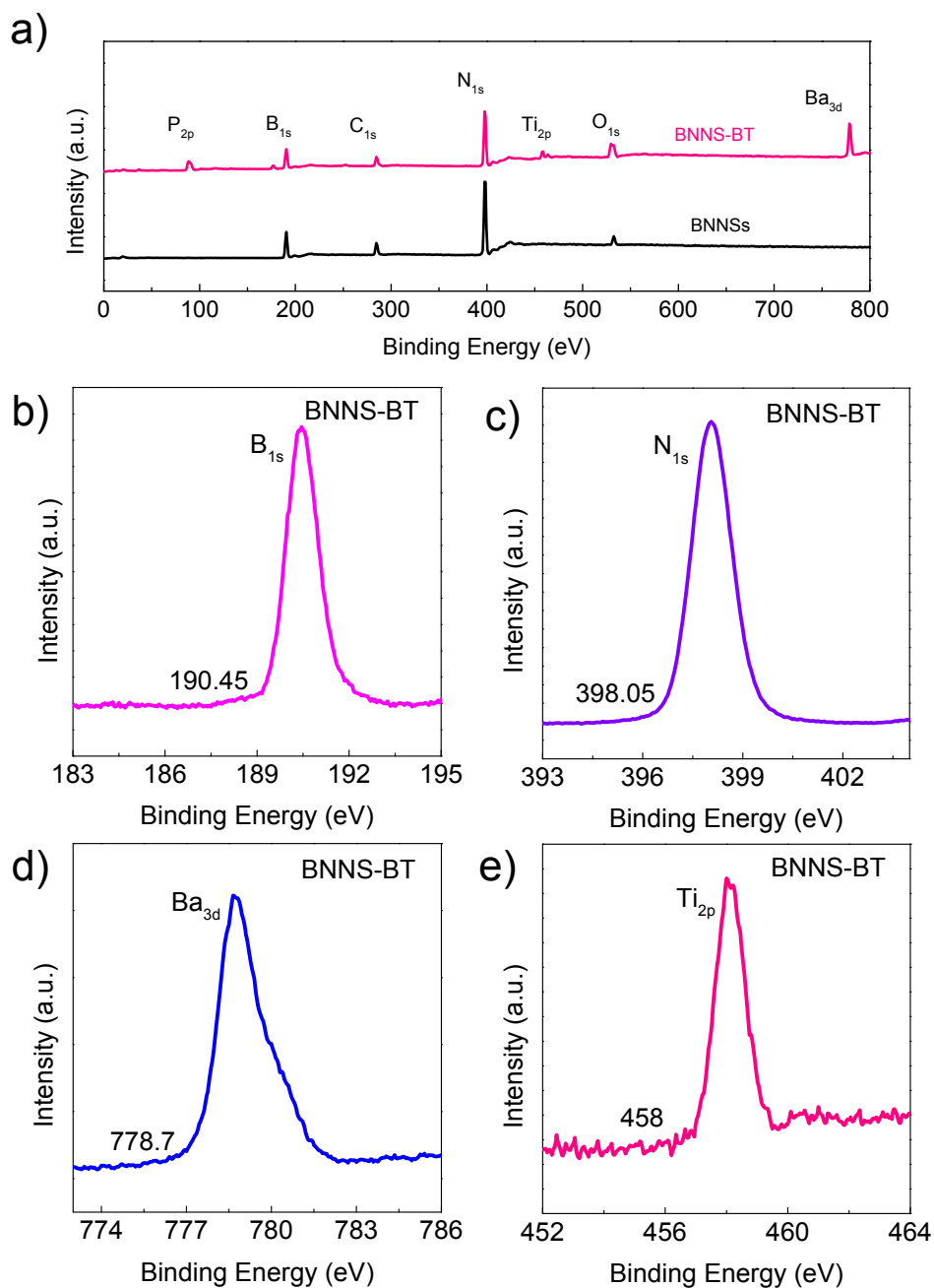


**Figure S6.** (a) XPS spectrum of BNNSs and BNNS-BT. Core level XPS spectra of (b) B<sub>1s</sub>, (c) N<sub>1s</sub>, (d) Ba<sub>3d</sub> and (e) Ti<sub>2p</sub> species in BNNS-BT.

## Calculation method of the grafting density

The grafting density of OPA can be continuously regulated by changing the reaction time and temperature, and the ratio of grafted BT and BNNSs in BNNS-BT can be further continuously regulated by changing the amount of BT and BNNSs. Two samples (Sample 1 and Sample 2) with different OPA grafting density were prepared, and their OPA grafting densities were calculated as  $0.33 \text{ nm}^{-2}$  and  $0.82 \text{ nm}^{-2}$ , respectively. Besides, two samples (Sample 1 and Sample 3) with the same OPA grafting density but different BT/BNNS ratios (i.e., 0.20 and 0.49) were also prepared.

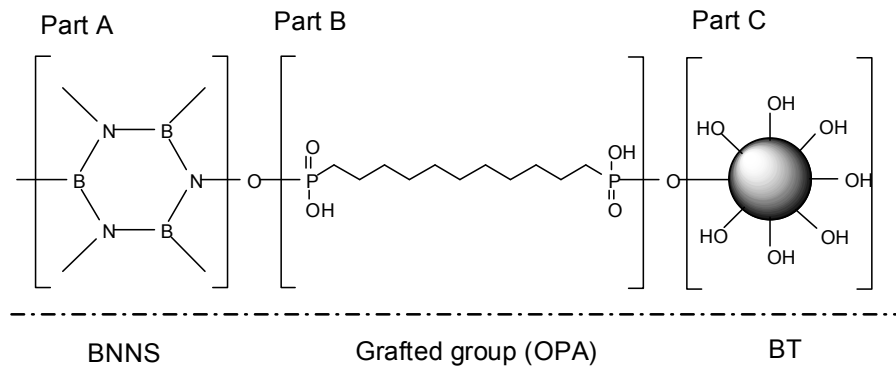


**Figure S7.** Structure of BNNS-BT

As is shown in **Figure S7**, since each B-N hexagonal ring contains three boron atoms and each grafted OPA group contains two phosphorus atoms, the graft density  $x$  (expressed as the number of grafted OPA groups per B-N hexagonal ring) for Sample 1 can be calculated by:

$$x = \frac{Atom(P) / 2}{Atom(B) / 3} = \frac{0.38 / 2}{31.75 / 3} = 0.018 \quad (1)$$

Given the diameter of one piece of BNNS is  $\sim 900 \text{ nm}$ , the surface area can be calculated by:

$$S_0 = 2 \times \pi \times \left(\frac{D}{2}\right)^2 = 1.272 \times 10^6 \text{ nm}^2 \quad (2)$$

The area of a single B-N hexagonal ring can be calculated by:

$$S_{h-BN} = 5.413 \times 10^{-2} \text{ nm}^2 \quad (3)$$

The number of B-N hexagonal rings on the surface of each BNNS can be calculated by:

$$n_{h\text{-BN}} = \frac{S_0}{S_{h\text{-BN}}} = \frac{1.272 \times 10^6}{5.413 \times 10^{-2}} = 2.36 \times 10^7 \quad (4)$$

The number of the grafted OPA groups on the surface of each BNNS can be calculated by:

$$n_{\text{OPA}} = x n_{h\text{-BN}} = 0.018 \times 2.36 \times 10^7 = 4.248 \times 10^5 \quad (5)$$

The OPA grafting density can be expressed as:

$$\frac{n_{\text{OPA}}}{S_0} = \frac{4.248 \times 10^5}{1.272 \times 10^6} = 0.33 \text{ nm}^{-2} \quad (6)$$

**Table S1** XPS analysis of BNNS-BT

	P (2p)	B (1s)	N (1s)	Ti (2p)	Ba (3d)	OPA grafting density	BT/BNNS ratio
BNNS-BT-1	0.38	31.75	28.86	0.83	0.49	0.33	0.20
BNNS-BT-2	1.38	46.96	38.4	2.48	1.94	0.82	0.82
BNNS-BT-3	0.45	42.64	35.19	1.96	1.65	0.33	0.49

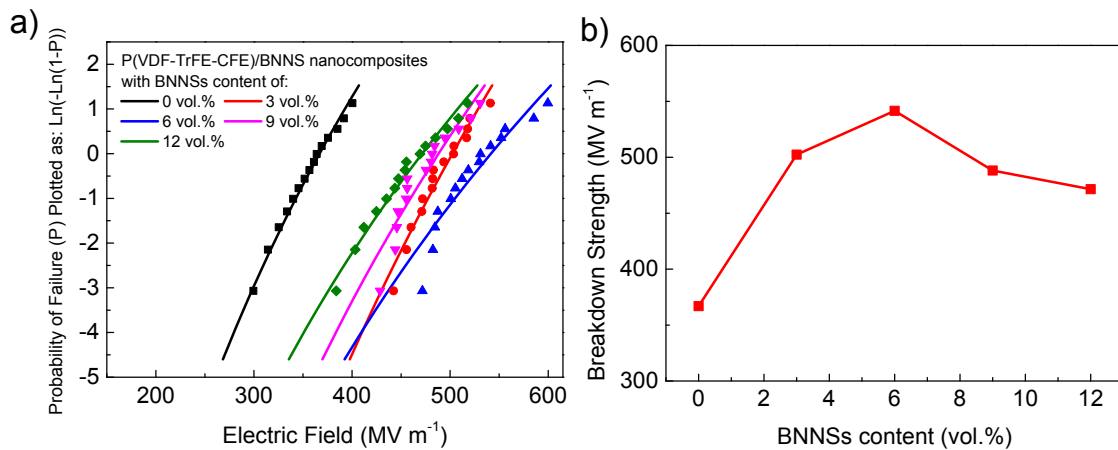


**Figure S8.** (a) Weibull plots of the breakdown strength of P(VDF-TrFE-CFE)/BNNS nanocomposites and (b) the characteristic breakdown strength as a function of BNNSs content.

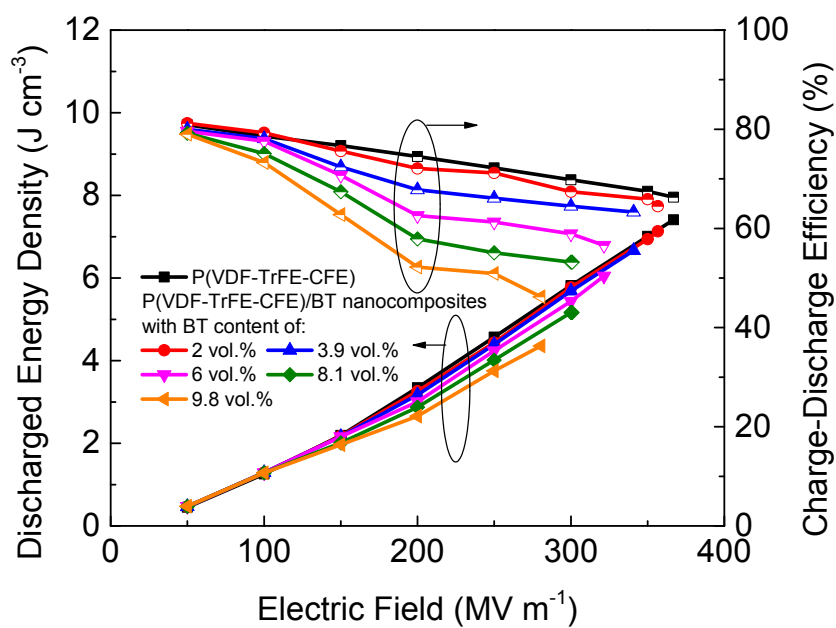


**Figure S9.** Discharged energy density and charge-discharge efficiency of P(VDF-TrFE-CFE)/BT nanocomposites with various content of BT.

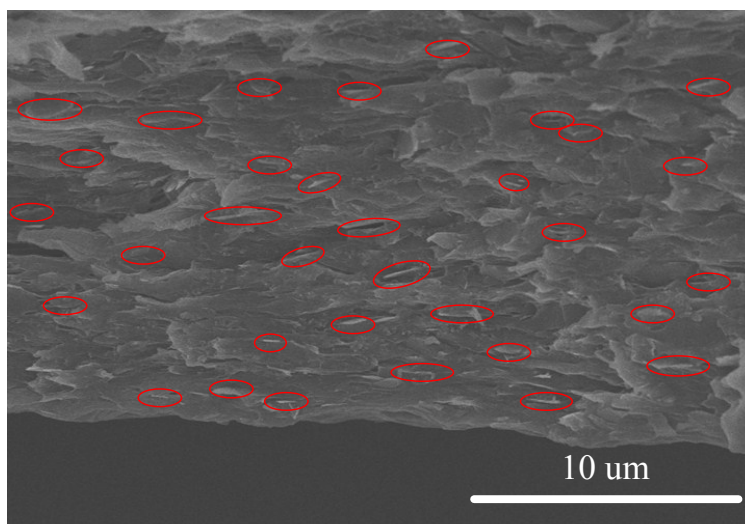


**Figure S10.** Cross-sectional SEM image of the P(VDF-TrFE-CFE)/BNNS-BT nanocomposites with 6 vol.% BNNSs and 3.9 vol.% BT.



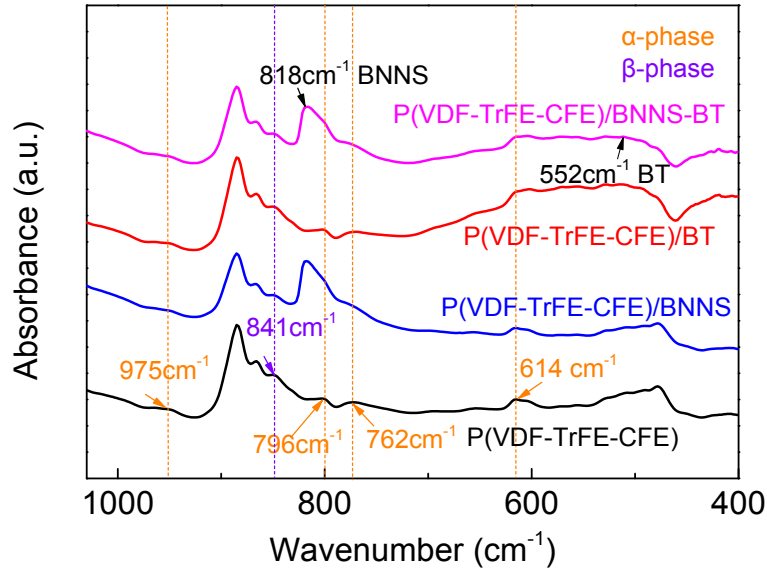


**Figure S11.** FTIR spectra of pristine P(VDF-TrFE-CFE), P(VDF-TrFE-CFE)/BNNS, P(VDF-TrFE-CFE)/BT and P(VDF-TrFE-CFE)/BNNS-BT. The absorption band at 550  $\text{cm}^{-1}$  is attributed to the stretching vibrations in the  $\text{TiO}_6$  octahedral of BT, and the absorption band at 818  $\text{cm}^{-1}$  belongs to BNNS. The absorption bands centered around 975  $\text{cm}^{-1}$ , 796  $\text{cm}^{-1}$ , 762  $\text{cm}^{-1}$ , 614  $\text{cm}^{-1}$  corresponding to the  $\text{TG}^+\text{TG}^-$  conformation in the  $\alpha$ -phase remain unchanged. The absorption band at 842  $\text{cm}^{-1}$  is ascribed to  $\text{T}_{n>3}\text{G}$  conformation in the  $\beta$ -phase. The absorption band at 614  $\text{cm}^{-1}$  corresponding to the  $\text{TG}^+\text{TG}^-$  conformation in the  $\gamma$ -phase is weak. The FTIR spectra indicates that the introduction of nanofillers does not change the crystal phase in P(VDF-TrFE-CFE), and there is not perceptible chemical interaction between the nanoparticles and the polymer matrix.

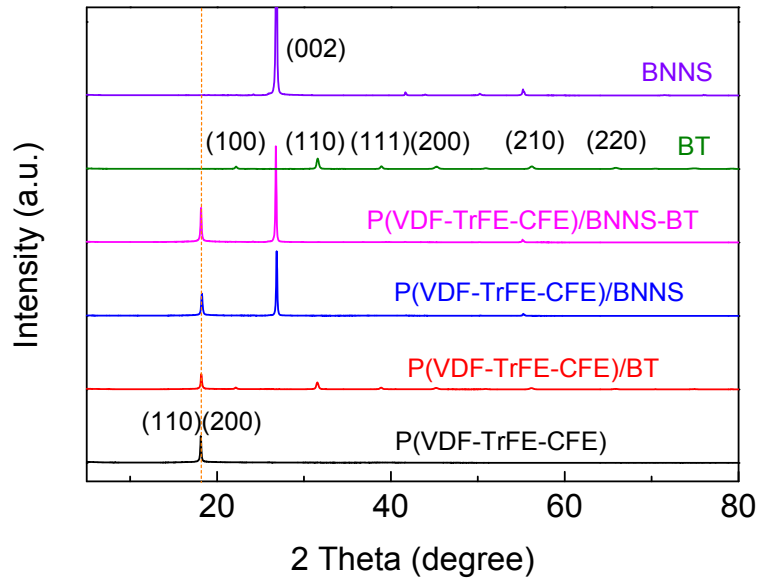


**Figure S12.** XRD patterns of the BNNS, BT, P(VDF-TrFE-CFE), P(VDF-TrFE-CFE)/BT nanocomposite with 3.9 vol.% BT, P(VDF-TrFE-CFE)/BNNS nanocomposite with 6 vol.% BNNS and P(VDF-TrFE-CFE)/BNNS-BT nanocomposite with 6 vol.% BNNS and 3.9 vol.% BT, where the peak at  $18.2^\circ$  is ascribed to (110)/(200) faces, indicating the nonpolar phase of P(VDF-TrFE-CFE) polymer, which is favorable for dipolar switching and thus inducing low ferroelectric loss.

**Table S2.** The mean size of crystallite for (110)/(200) faces of pristine P(VDF-TrFE-CFE) and the nanocomposites, from the XRD results.

Filler	FWHM	2 Theta	Mean size of the crystallite (nm)
0 vol.% BNNS+0 vol.% BT	0.171	18.122	49.16
0 vol.% BNNS+3.9 vol.% BT	0.187	18.234	44.08
6 vol.% BNNS+0 vol.% BT	0.198	18.241	41.59
6 vol.% BNNS+3.9 vol.% BT	0.186	18.262	44.13

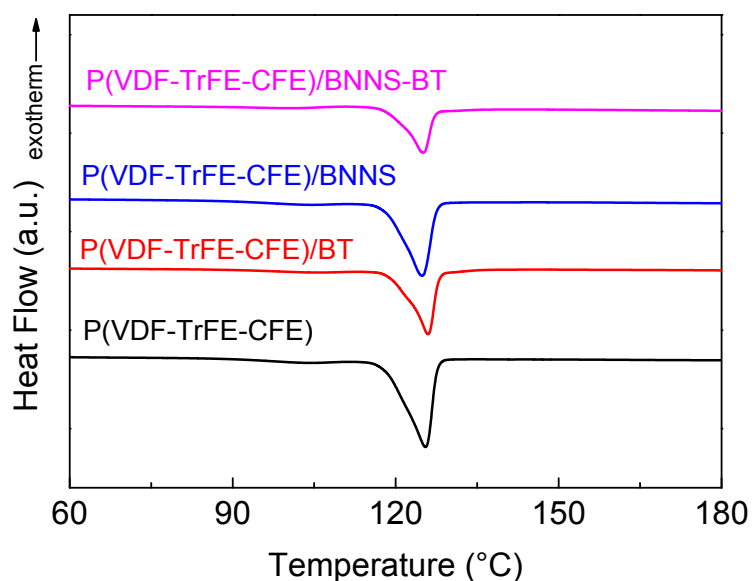


**Figure S13.** DSC curves of pristine P(VDF-TrFE-CFE), P(VDF-TrFE-CFE)/BNNS, P(VDF-TrFE-CFE)/BT and P(VDF-TrFE-CFE)/BNNS-BT.

**Table S3.** Crystalline temperature ( $T_c$ ) and crystallinity of pristine P(VDF-TrFE-CFE), P(VDF-TrFE-CFE)/BNNS, P(VDF-TrFE-CFE)/BT and P(VDF-TrFE-CFE)/BNNS-BT, from DSC results.

Filler	$T_c$ (°C)	Crystallinity (%)
0 vol.% BNNS+0 vol.% BT	125.5	27.10%
0 vol.% BNNS+3.9 vol.% BT	125.7	26.10%
6 vol.% BNNS+0 vol.% BT	125.2	26.50%
6 vol.% BNNS+3.9 vol.% BT	125.3	25.80%